

# *In vivo* ultrahigh-resolution optical coherence tomography

W. Drexler, U. Morgner, F. X. Kärtner, C. Pitris, S. A. Boppart, X. D. Li, E. P. Ippen, and J. G. Fujimoto

Department of Electrical Engineering and Computer Science and Research Laboratory of Electronics,  
Massachusetts Institute of Technology, Cambridge, Massachusetts 02139

Received April 28, 1999

Ultrahigh-resolution optical coherence tomography (OCT) by use of state of the art broad-bandwidth femtosecond laser technology is demonstrated and applied to *in vivo* subcellular imaging. Imaging is performed with a Kerr-lens mode-locked Ti:sapphire laser with double-chirped mirrors that emits sub-two-cycle pulses with bandwidths of up to 350 nm, centered at 800 nm. Longitudinal resolutions of  $\sim 1 \mu\text{m}$  and transverse resolution of  $3 \mu\text{m}$ , with a 110-dB dynamic range, are achieved in biological tissue. To overcome depth-of-field limitations we perform zone focusing and image fusion to construct a tomogram with high transverse resolution throughout the image depth. To our knowledge this is the highest longitudinal resolution demonstrated to date for *in vivo* OCT imaging. © 1999 Optical Society of America

OCIS codes: 170.4500, 170.3880, 120.3180, 110.6960, 320.7090, 140.4050.

Optical coherence tomography (OCT) can be used to perform high-resolution cross-sectional *in vivo* and *in situ* imaging of microstructure in transparent<sup>1</sup> as well as nontransparent<sup>2</sup> biological tissue. The parameters that govern OCT performance are longitudinal and transverse resolution, dynamic range, measurement speed, and the center wavelength of the light source. The longitudinal resolution, governed by the coherence length, is inversely proportional to the optical bandwidth of the light source.<sup>3</sup> Superluminescent diodes (SLD's) are often used for OCT imaging and typically have 10–15- $\mu\text{m}$  longitudinal resolution. This resolution is insufficient for identifying individual cells or assessing subcellular structures such as nuclei. Cellular-level resolutions would improve imaging of early neoplastic changes for cancer screening as well as permit new applications in developmental biology. Ultrahigh-resolution OCT would also improve the sensitivity and specificity of diagnosis of ocular diseases. The first sub-10- $\mu\text{m}$ -resolution low-coherence interferometry was achieved by use of broadband fluorescence from an organic dye<sup>4</sup> and from Ti:sapphire.<sup>5</sup> However, OCT could not be performed owing to low brightness. Retinal tomograms with a resolution of 7–8  $\mu\text{m}$  in free space at 800 and 1300 nm were demonstrated by multiplexing of spectrally displaced SLD's.<sup>6,7</sup> OCT imaging *in vitro* with resolution of 3.7  $\mu\text{m}$  at 800 nm (Ref. 8) and *in vivo* with 5.1  $\mu\text{m}$  at 1300 nm (Ref. 9) was recently demonstrated with Kerr-lens mode-locked (KLM) solid-state lasers.

In this Letter we present an ultrahigh-resolution OCT system that uses state of the art broad-bandwidth femtosecond laser technology. We demonstrate *in vivo* subcellular imaging with longitudinal resolution of  $\sim 1 \mu\text{m}$  in tissue, to our knowledge the highest longitudinal resolution OCT achieved to date. A zone-focusing and image-fusion technique, similar to ultrasound C-mode scanning,<sup>10</sup> is demonstrated to overcome depth-of-field limitations.

The OCT system presented in this study uses a KLM femtosecond Ti:sapphire laser that emits sub-two-cycle pulses, corresponding to bandwidths of up to 350 nm (FWHM) at 800 nm.<sup>11</sup> To our knowledge these pulses are the shortest ever generated directly from a laser

oscillator. This high performance is achieved with specially designed double-chirped mirrors with a high-reflectivity bandwidth and a controlled dispersion response, in combination with low-dispersion calcium fluoride prisms for intracavity dispersion compensation. A pair of fused-silica prisms and razor blades are used to spectrally disperse the laser beam and spectrally shape the laser output.

The OCT system must be optimized to accommodate the ultrabroad bandwidth of the Ti:sapphire laser (Fig. 1). Specially designed objectives (CL's and OL, optimized for a bandwidth from 600 to 1000 nm) with a 10-mm focal length and a numerical aperture of 0.30 in combination with single-mode fibers (570-nm cutoff wavelength) and special broadband 3-dB fiber couplers (FC's) were used to maintain ultrabroad-bandwidth and single-mode propagation. Both chromatic aberration and group-velocity dispersion can degrade longitudinal resolution. The interferogram is broadened if there is a significant group-velocity dispersion mismatch between the reference and the sample arm. Polarization mismatch also degrades the shape and the peak height of the interference envelope, so polarization controllers (PC's) were used. Dispersion is matched by use of variable-thickness fused-silica (FS) and BK7 prisms until a uniform group-delay dispersion is achieved by calculation and display of the phase

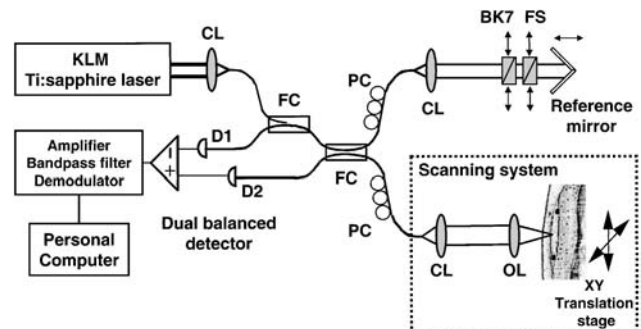


Fig. 1. Ultrahigh-resolution fiber OCT system with a KLM mode-locked Ti:sapphire laser. The interferometer is dispersion balanced and optically and electronically optimized to support broad optical bandwidths. See text for definitions.

of the fast Fourier transform of the interference signal from a mirror in real time. To minimize higher-order dispersion effects we used FS to compensate for fiber-length differences and BK7 to compensate for optical-material mismatch in the interferometer. In contrast with SLD's, the Ti:sapphire laser has excess amplitude noise, caused mainly by the argon-ion pump laser, which decreases the signal-to-noise performance. Nevertheless, a nearly shot-noise-limited sensitivity can be obtained by use of dual balanced detection (D1, D2, detectors). A neutral-density 3.0 filter followed by a mirror was used as a calibration sample with 50-dB reflectivity. A system sensitivity of 110 dB was obtained. We used a passive second-order Butterworth bandpass filter with a quality factor  $Q \sim 3-4$ .

The ultrahigh-resolution OCT system was optimized to support optical spectra of up to 260 nm (FWHM), and a 1.5- $\mu\text{m}$  longitudinal resolution in free space was achieved, corresponding to  $\sim 1 \mu\text{m}$  in tissue (Fig. 2). This is in good agreement with the value of 1.4  $\mu\text{m}$  calculated from the fast Fourier transform of the optical spectrum. Because the spectrum is not perfectly Gaussian shaped, sidelobes in the interferometric autocorrelation appear at  $\pm 1.8 \mu\text{m}$  with  $-15\text{-dB}$  magnitude. The resolution achieved here is more than a factor of 7 better than with SLD's, which have 32-nm (FWHM) optical bandwidth and 11.5- $\mu\text{m}$  resolution. To achieve high transverse resolution we used a specially designed achromatic doublet with 10-mm focal length (OL). In the sample arm the fiber core ( $\sim 4 \mu\text{m}$ ) is imaged onto the sample by the collimating lens (CL) and the objective lens (OL) (Fig. 1). By changing the position of the collimating lens (CL), we can vary the transverse resolution from 3 to 5  $\mu\text{m}$ , with a corresponding confocal parameter of 35 to 100  $\mu\text{m}$  in air. We measured the beam diameter by recording the intensity profile while moving a razor blade through the beam in 0.25- $\mu\text{m}$  steps and fitting an error function.

The feasibility of *in vivo* subcellular imaging was demonstrated by use of a well-established developmental biology animal model, the African frog tadpole (*Xenopus laevis*). Figure 3 shows an *in vivo* OCT image of a 28-day-old anesthetized specimen. We kept the tadpole in tank water in a clay-linked Petri dish to prevent it from dehydrating and to provide index matching. To minimize wave-front aberration and achieve optimal transverse resolution we placed a 130- $\mu\text{m}$ -thick microscope cover glass on top of the immersed specimen. The incident power was 1 mW. Figure 3 shows an area of 0.75 mm  $\times$  0.5 mm imaged at  $\sim 1 \mu\text{m} \times 3 \mu\text{m}$  (longitudinal  $\times$  transverse) resolution and consisting of 1700  $\times$  1000 pixels. Tissue morphology, including the neural olfactory tract, as well as pleomorphic mesenchymal cells can be visualized. Cell membranes and cell nuclei appear highly backscattering compared with the weakly scattering cytoplasm. OCT can image nuclear and intracellular morphology as well as identify cells in different stages of mitosis and visualize mitotic activity (see the two cell pairs indicated by arrows in Fig. 3). Owing to the high transverse resolution, the confocal parameter is only 35  $\mu\text{m}$  in air, resulting in image degradation outside of the focused zone. To overcome this

depth-of-field limitation and maintain high transverse resolution at varying depths through the image we used a zone-focusing and image-fusion technique. We constructed Fig. 3 by manually segmenting and fusing nine separate images recorded with different focal depths of the optics, while maintaining the same interferometer delay depth (1 mm). This technique is similar to C-mode scanning used in ultrasound imaging.<sup>10</sup> We obtained as much as 80–100- $\mu\text{m}$  imaging depth from each recorded tomogram without significant image degradation. We also measured the depth of field experimentally by imaging polystyrene microspheres in gel. No readjustment of the dispersion compensation for each focusing position was necessary, since the measured FWHM of single A-scan peaks revealed no depth-dependent dispersion over a distance of 0.75 mm. Four representative images are indicated in Fig. 4, each recorded over  $\sim 0.54 \text{ mm} \times 0.5 \text{ mm}$  with  $\sim 1 \mu\text{m} \times 3 \mu\text{m}$  (longitudinal  $\times$  transverse) resolution and consisting of 1200  $\times$  1000 pixels. Dynamic focus tracking can also be used to maintain high transverse resolution at different focal depths, but this technique requires rapid scanning of a lens and setting the focal depth coincident with the interferometer zero delay.<sup>7,12</sup>

In conclusion, *in vivo* OCT imaging with  $\sim 1\text{-}\mu\text{m}$  longitudinal resolution was demonstrated by use of ultrabroad-bandwidth femtosecond laser technology.

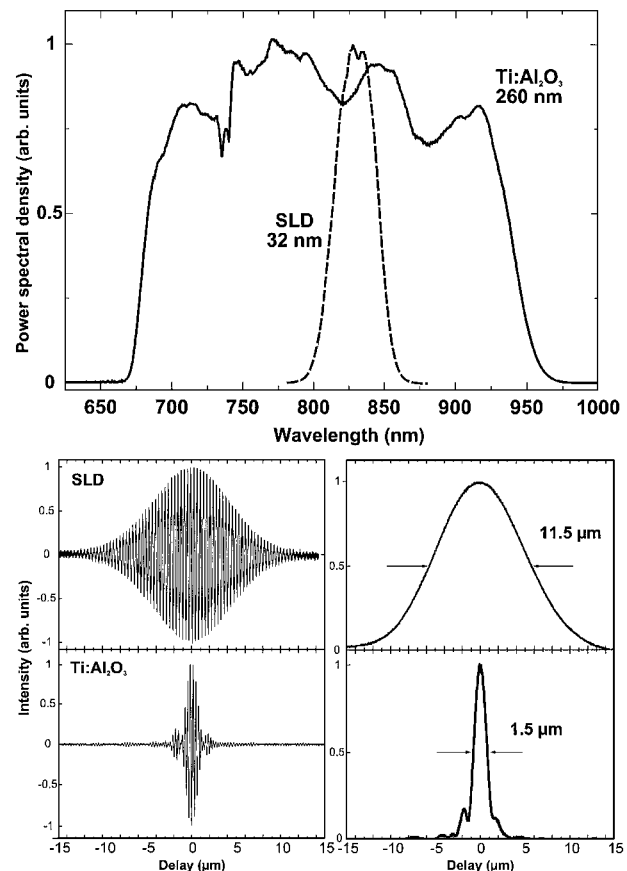


Fig. 2. Optical output spectrum (top), interference signals and envelopes (middle and bottom) of the KLM Ti:sapphire laser versus a SLD. An optical bandwidth of 260 nm permits a free-space resolution of 1.5  $\mu\text{m}$  for the laser, compared with 32-nm and 11.5- $\mu\text{m}$  resolution with a SLD.

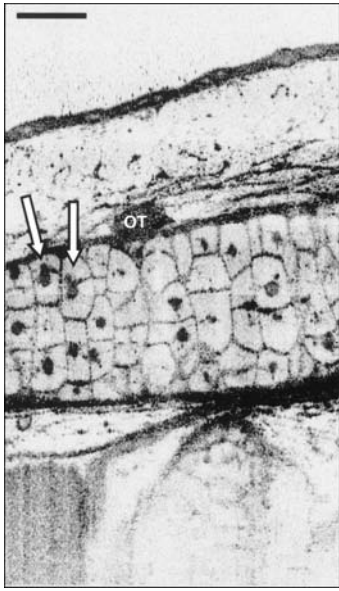


Fig. 3. *In vivo* subcellular level resolution ( $1\ \mu\text{m} \times 3\ \mu\text{m}$ , longitudinal  $\times$  transverse) tomogram of an African frog tadpole (*Xenopus laevis*). Multiple mesenchymal cells of various sizes and nuclear-to-cytoplasmic ratios, olfactory tract (OT) and intracellular morphology, as well as mitosis of two cell pairs (arrows), are clearly shown. Bar:  $100\ \mu\text{m}$ .

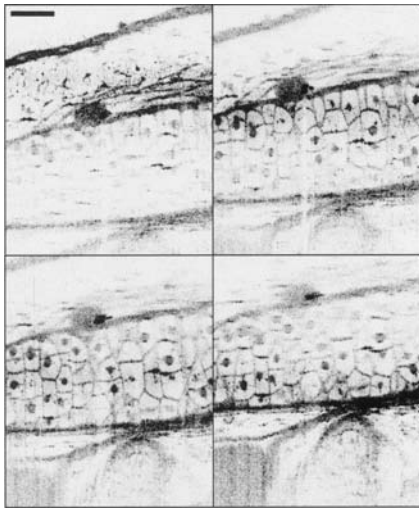


Fig. 4. *In vivo* ultrahigh-resolution ( $1\ \mu\text{m} \times 3\ \mu\text{m}$ , longitudinal  $\times$  transverse) tomograms of the same site of an African frog tadpole (*Xenopus laevis*), recorded with different depths of focus. We fused these images, in addition to five others, to construct the image shown in Fig. 3 to maintain high transverse resolution throughout the depth that was imaged. Bar:  $100\ \mu\text{m}$ .

To our knowledge, this is the highest OCT resolution imaging performed to date. *In vivo* imaging of human cells, typically of the order of  $10\ \mu\text{m}$ , should be possible with this system. High-resolution OCT has important implications for early cancer diagnosis. Imaging depths of 0.5–1.0 mm can be achieved in

nontransparent tissue at this wavelength. Light at 800 nm has the advantage that it is not strongly absorbed by water, so retinal structures can be imaged even through  $\sim 25$  mm of ocular media. This capability would permit high-resolution *in vivo* retinal imaging and improve the diagnosis of diseases, including glaucoma and macular edema. The broad bandwidth that is available from this system should also permit spectroscopic OCT imaging for measurement of spatially localized, wavelength-dependent scattering and absorption.

We gratefully acknowledge contributions from E. Swanson of Coherent Diagnostic Technology, M. Brezinski, S. H. Cho of the Massachusetts Institute of Technology (MIT), and Hazel Sive and her laboratory at MIT for providing specimens. W. Drexler gratefully acknowledges support from Max Kade Foundation, Inc., and the Österreichische Akademie der Wissenschaften, and U. Morgner and F. X. Kärtner acknowledge support from the Deutsche Forschungsgemeinschaft. This research was supported in part by U.S. Air Force Office of Scientific Research contract F4920-98-1-0139, U.S. Office of Naval Research Medical Free Electron Laser Program contract N000014-97-1-1066, and National Institutes of Health contracts NIH-9-RO1-CA75289-02 and NIH-9-RO1-EY11289-14.

## References

1. D. Huang, E. Swanson, C. P. Lin, J. S. Schuman, W. G. Stinson, W. Chang, M. R. Hee, T. Flotte, K. Gregory, C. A. Puliafito, and J. G. Fujimoto, *Science* **254**, 1178 (1991).
2. J. G. Fujimoto, M. E. Brezinski, G. J. Tearney, S. A. Boppart, B. E. Bouma, M. R. Hee, J. F. Southern, and E. A. Swanson, *Nature Med.* **1**, 970 (1995).
3. E. A. Swanson, D. Huang, M. R. Hee, J. G. Fujimoto, C. P. Lin, and C. A. Puliafito, *Opt. Lett.* **17**, 151 (1992).
4. H. H. Liu, P. H. Cheng, and J. Wang, *Opt. Lett.* **18**, 678 (1993).
5. X. Clivaz, F. Marquis-Weible, and R. P. Salathé, *Electron. Lett.* **28**, 1553 (1992).
6. A. Baumgartner, C. K. Hitzenberger, H. Sattmann, W. Drexler, and A. F. Fercher, *J. Biomed. Opt.* **3**, 45 (1998).
7. J. M. Schmitt, S. L. Lee, and K. M. Yung, *Opt. Commun.* **142**, 203 (1997).
8. B. E. Bouma, G. J. Tearney, S. A. Boppart, M. R. Hee, M. E. Brezinski, and J. G. Fujimoto, *Opt. Lett.* **20**, 1486 (1995).
9. S. A. Boppart, B. E. Bouma, C. Pitris, J. F. Southern, M. E. Brezinski, and J. G. Fujimoto, *Nature Med.* **4**, 861 (1998).
10. M. D. Sherar, M. B. Noss, and F. S. Foster, *Nature* **330**, 493 (1987).
11. U. Morgner, F. X. Kärtner, S. Cho, Y. Chen, H. A. Haus, J. G. Fujimoto, E. P. Ippen, V. Scheurer, G. Angelow, and T. Tschudi, *Opt. Lett.* **24**, 411 (1999).
12. F. Lexer, C. K. Hitzenberger, W. Drexler, S. Molebny, H. Sattmann, M. Sticker, and A. F. Fercher, *J. Mod. Opt.* **46**, 541 (1999).